FREQUENCY AND NON-LINEAR ANALYSIS OF BUBBLE PATHS IN BUBBLE CHAIN

Romuald MOSDORF*, Tomasz WYSZKOWSKI[*]

[*]Bialystok Technical University, Faculty of Mechanical Engineering, ul. Wiejska 45, 15-351 Bialystok, Poland

r.mosdorf@pb.edu.pl, wyszkowski.tomasz@gmail.com

Abstract: In the paper the paths of bubbles emitted from the bras nozzle with inner diameter equal to 1.1 mm have been analyzed. The mean frequency of bubble departure was in the range from 1 to 36 Hz. Bubble paths have been recorded using a high speed camera. The image analysis technique has been used to obtain the bubble paths for different mean frequencies of bubble departures. The Fourier, wavelet analysis and recurrence plots have been used to determine the strength of interaction between bubbles in column. It has been found that the influence of previously departing bubbles on trajectory of next bubble in the column can be significant for $f_b > 30$ Hz, in this case the bubble paths become less periodic and more instable. In this case the distance between subsequent departing bubbles (S/D) becomes close to 1. It causes that the vertical interaction between departing bubbles is enough strong to change the dynamical properties of bubble paths.

1. INTRODUCTION

The knowledge of bubble dynamics is of key importance in physical, biological and medical processes, and particularly in industrial applications. There are numerous physical parameters such as: physical properties of the two phases, gas flow rate, gas pressure, height of the liquid and gravity conditions which influence on the bubbles formation. Hence, most of efforts have been devoted to the formation of bubbles from single nozzles or orifice plates. The study of bubble dynamics is crucial to understand bubble-liquid and bubble-bubble interactions. According to Luewisutthichat et al. (1997) the bubble motion and bubble shape are controlled by deterministic forces such as body force and drag force caused by the convective motion, and the complex non-linear forces generated by liquid motion around bubbles. Results of investigation show that such quantity as: bubble departure frequency (time between subsequent departing bubbles), bubble departure diameter, bubble shape and its deformation, gas pressure fluctuation in the nozzle, bubbles interaction, bubbles coalescence and bouncing, structure of liquid flow around the bubbles and bubble column change in time chaotically (Mosdorf and Shoji, 2003; Zhang and Shoji, 2003; Kikuchi et al., 1997; Femat et al., 1998; Vazquez at al., 2008).

The tubes of streamwise liquid vorticity are being left by each bubble and they are responsible for appearance of lift force acting on the bubbles (Zenit and Magnaudet, 2009). The strength of the circulation of each vortex tubes decreases with increase in the distance from the bubble. The bubbles in the bubble column create the complex structure of bubble wakes. These wakes interact between each others and finally modify the bubbles trajectory. The increase of bubble departure frequency decreases the vertical distance between bubbles. It causes the increase of interaction between the bubbles and tubes of streamwise liquid vorticity generated by previously bubbles. Such interaction changes the lift force and finally modify the oscillation bubble trajectory.

In the present paper the dynamical properties of bubble paths have been investigated to detect the strength of interaction between bubbles. The paths of bubbles emitted from the bras nozzle with inner diameter equal to 1.1 mm has been analyzed. The bubble departure diameter was ~4.5 mm. The laser-photodiode system has been used to measure the frequency of bubble departures. The analyzed frequencies ranged from 1 to 36 Hz (bubbles per second). The bubble paths have been recorded using a high speed camera. The image analysis technique enabled us to obtain the 2D bubble paths for different mean frequencies of bubble departures. The Fourier analysis, wavelet analysis and recurrence plots have been used to determine the strength of interaction between bubbles.

2. EXPERIMENTAL SETUP AND BUBBLE BEHAVIOURS

The air bubble paths in bubble column in the tank (400 x 500 x 40 mm) filled with distillated water has been investigated. In the experiment bubbles were generated from the brass nozzle with inner diameter of 1.1 mm.

Because in the experiment with bubble column generation both the pressure and gas mass flux fluctuated then in order to evaluate experiment conditions it was necessary to use the mean value of gas mass flux or bubble departure frequency. In the present experiment the mean bubble departure frequency was used as a control parameter. The frequency has been measured using simultaneously the laser - phototransistor system and gas pressure sensor. The gas pressure fluctuation has been measured using uncompensated silicon pressure sensor MPX12DP. In the laser-phototransistor system the semiconductor red laser with wave length of 650 nm, 3mW, special aperture and phototransistor BPYP22 has been used. The diameter

of laser ray was 0.2 mm. The experiment has been carried out in conditions when subsequent departing bubbles did not coalesce vertically close to the nozzle outlet. The frequency of bubble departure was in the range from 2 to 36 bubbles per second, the water temperature was 20°C.

All data was simultaneously recorded using the data acquisition system DT9800 series USB Function Modules for Data Acquisition Systems with sampling frequency of 1000 Hz. The air supply system consisted of air tank capacity of 2 dm^3 and the electronically controlled air pump, where the velocity of electric engine was controlled by the chip U2008B. The scheme of experimental stand has been shown in Fig. 1.

Bubble paths have been recorded in the rectangle area of 230 x 50 mm using the high speed camera Casio EX FX1. The recorded color video (600 fps) has been divided into frames. All colored frames were converted into gray scale images. The Sobel filter based on convolution of the image with a small, integer valued filter has been used to identify the bubbles on the frames (Hedengren, 1988). Exemplary results of using the Sobel filter for bubble image are presented in Fig. 2a. Because the Sobel algorithm identifies only the edge of the bubble, therefore the additional algorithm to fill interior of the detected bubble by black pixels has been used. Finally, each bubble was visible in the frame as a set of black pixels (Fig. 2).

The path of each bubble was reconstructed by tracking the trajectory of mass center of each bubble in subsequent frames. The mass centre has been calculated according to the following formula:

$$x_c = \frac{\Sigma_i \Sigma_j k}{S} \tag{1}$$

where $k = \begin{cases} i \; for \; black \; pixels \\ 0 \end{cases}$

$$y_c = \frac{\Sigma_i \Sigma_j k}{S} \tag{2}$$

where $k = \begin{cases} j \; for \; black \; pixels \\ 0 \end{cases}$

where S – the area of the bubble picture.

In the paper the paths of bubbles which do not coalesce with another bubbles have been analyzed.

In Fig. 3 it has been shown the data recorded from the phototransistor and pressure sensor for different mean frequencies of bubble departures. The laser ray passed 3 mm above the nozzle outlet. When the bubble was passing through the laser ray the phototransistor sensor generated the signal of the low voltage level. The time between bubbles is visible in Fig. 3 as a signal of the high voltage level. Obtained results show that for all frequencies of bubble departures the time periods in which the bubbles pass through the laser ray are approximately the same and are equal to 0.018 ±0.002 [s], but mean time periods between subsequent departing bubbles decrease together with increase of bubble departure frequencies as it has been shown in Fig. 4.

When bubbles depart, the air pressure rapidly decreases as it has been shown in Fig. 3. The number of minimums of pressure signal and number of periods with low voltage level signal coming from phototransistor sensor have been used to determine bubble departure frequencies.

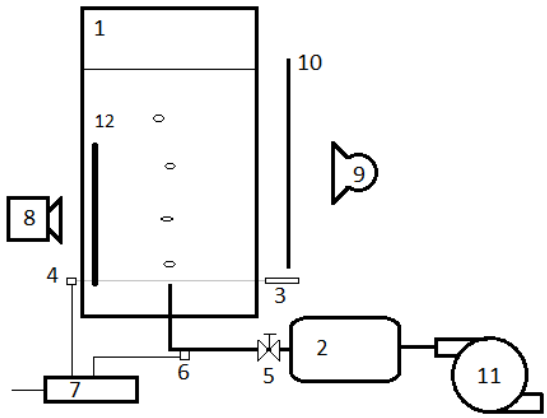

Fig. 1. Experimental setup. 1 – glass tank, 2 – air tank, 3 – laser, 4 – phototransistor, 5 – air valve, 6 – pressure sensor, 7 – computer acquisition system (DT9800 series USB Function Modules for Data Acquisition Systems), 8 – Casio EX FX1(600 fps), 9 – light source, 10 – screen, 11 – air pump with electronic control, 12 – The rectangle area of 230x50 mm where the bubble paths has been recorded

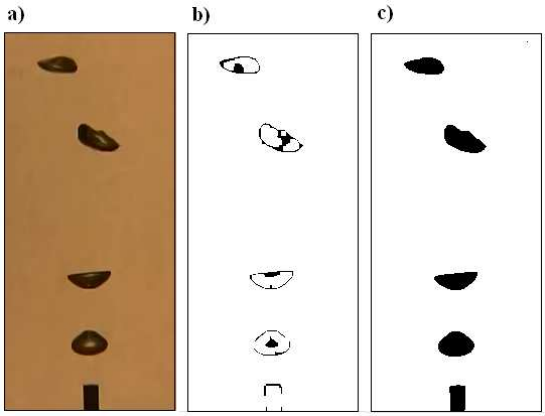

Fig. 2. The bubble identification process. a) original photo. b) results of Sobel filter, c) filling interior of the bubbles by black pixels

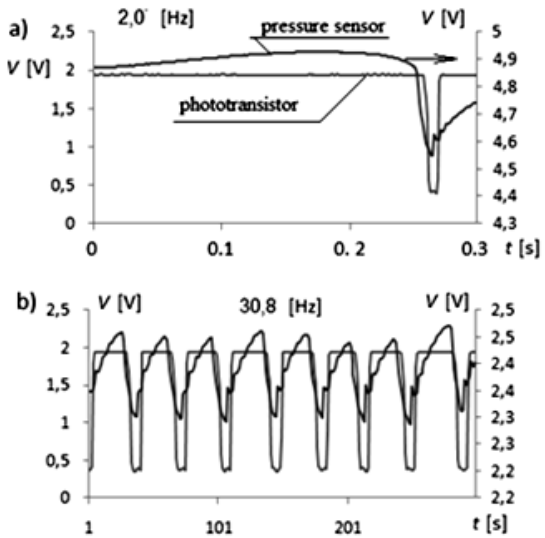

Fig. 3. Pressure and phototransistor signal recorded for different frequencies of bubble departures f_b a) f_b = 2 Hz, b) f_b = 30.08 Hz

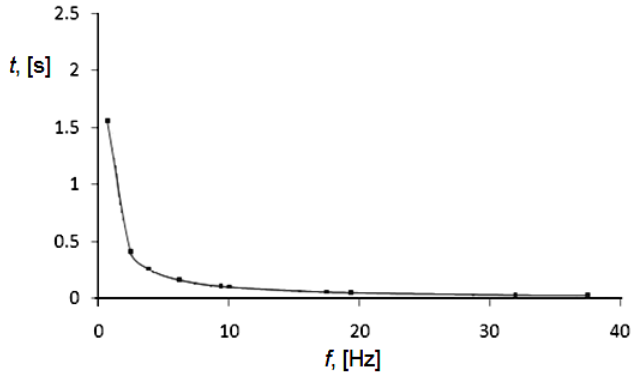

Fig. 4. The mean time periods between subsequent departing

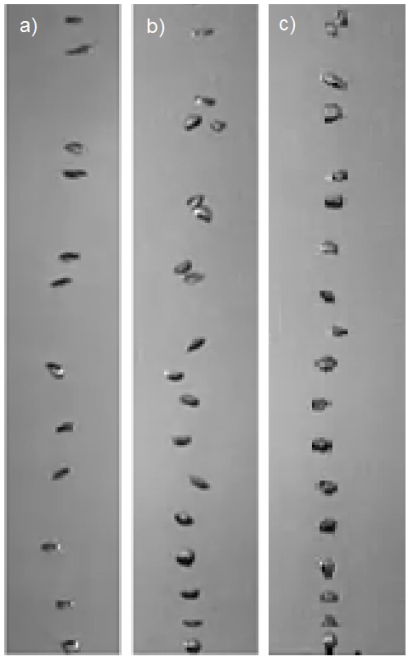

Fig. 5. The changes in time of the horizontal position of the bubble and the typical behavior of bubble flow for different mean bubble departure frequencies f_b a) f_b = 14.4 [Hz], b) f_b = 30 [Hz], c) f_b = 36 [Hz]

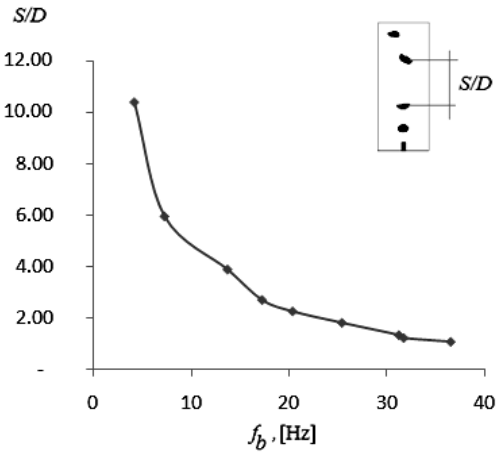

Fig. 6. Estimated distance between subsequent bubbles

In Fig. 5 the typical behavior of bubble flow for different mean bubble departure frequencies has been presented. Changes of frequency of bubble departures cause the changes of average distance between bubbles in the bubble chain. The distance has been measured between two subsequent bubbles when the lower bubble was 10 mm over the nozzle outlet. In Fig. 6 it has been shown the distance between bubbles vs frequency of bubbles departure.

3. ANALYSIS OF FREQUENCY OF BUBBLE DEPARTURES

One of the main problem in investigation of bubbling flow is an analysis of frequency of bubble departure. Such frequency can be constant in time (bubbles depart periodically) or change chaotically in time (bubbles depart chaotically). The Fourier transformation allows us to represent the time-domain data in the frequency domain. The Fourier power spectrum answers the question which frequencies contain the signal power. The answer has a form of distribution of power values as a function of frequency. In the frequency domain, this is the square of Fourier transformation. For the measurement data in the form of discrete series x_n the Fourier transformation has a following form:

$$F_k = \sum_{n=0}^{N-1} x_n e^{-j\frac{2\pi}{N}kl} \tag{3}$$

The power spectrum is defined as $P = |F_k|^2$. The examples of power spectrums of data recorded in the experiment have been shown in Fig. 7.

Obtained results for bubble paths have been compared with results of analysis prepared for the test path described by the function $\mathrm{x}(t) = \ln(t) \cdot \sin(\omega t)$. Power spectrum of test path has been shown in Fig. 7c. In this case the dominant frequency is equal to bubble path oscillation frequency - 4.63 [Hz]. The power spectrum presented in Fig. 7c is characteristic for periodic system. Power spectrums obtained for experimental data presented in Fig. 7.a,b are characteristic for deterministic chaos system.

In case when f_b = 0.9 [Hz] (Fig. 7a) the bubble path oscillation frequency is a dominant frequency of power spectrum and is equal to 4.87 [Hz]. But in power spectrum we can distinguish the additional frequencies with relatively high amplitudes. These frequencies are connected with trends of bubble paths. Together with the increase of frequency of bubble departures the amplitudes of these additional frequencies (less than 5 [Hz]) increase, which is presented in Fig. 7b. It means that bubble paths become more unstable.

The Fourier power spectrum does not allow us to identify the frequency changes in time. This problem can be analyzed using the windowed Fourier transformation (Torrence and Compo, 1998, 2005), but this is an inaccurate method to localize time–frequency. The method which eliminates this inaccuracy is the wavelet analysis. It is a tool for analyzing the localized variations of power spectrum within the time series x_n, with equal time spacing δt (Torrence and Compo, 1998, 2005). The continuous wavelet transformation of a discrete sequence x_n is defined as the convolution of x_n with a scaled wavelet Ψ (Torrence and Compo, 1998, 2005):

$$W(t,s)=\sum_{t'=0}^{N-1} x_{t'}\Psi^{*}\left[\frac{(t'-t)\delta t}{s}\right] \tag{4}$$

where (*) indicates the complex conjugate.

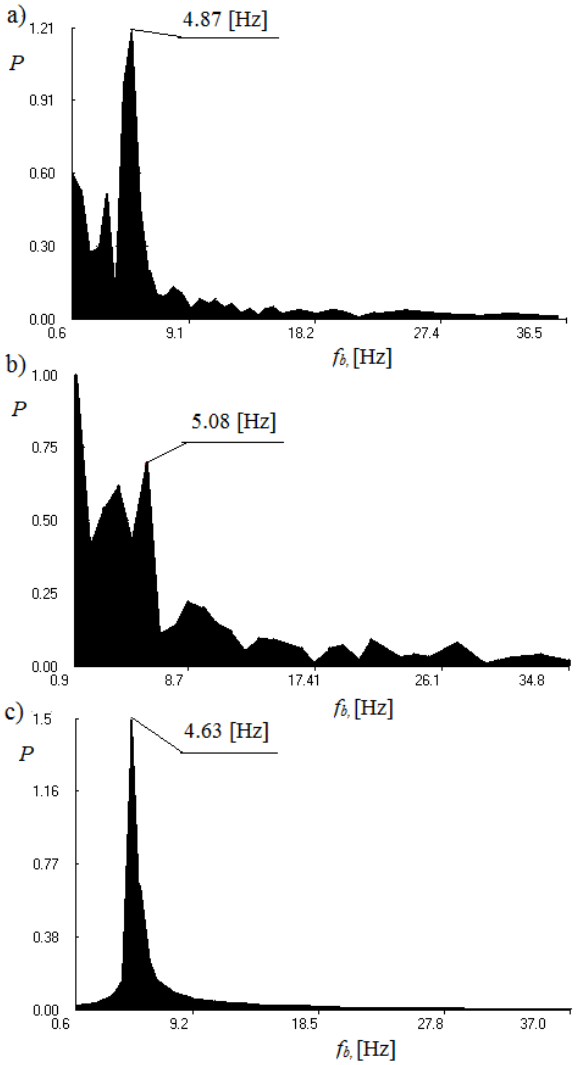

Fig. 7. Fourier power spectrums for different frequencies of bubble departures f_b. a) f_b = 0.9 Hz, b) f_b = 36.5 Hz, c) Test path

Because the wavelet function $\Psi_o(\eta)$ is generally complex, the wavelet transformation $W(t,s)$ is also complex. The wavelet power spectrum is defined as: $|W(t,s)|^2$ (Torrence and Compo, 1998, 2005).

In the analysis the Morlet wavelet has been used as the based wavelet and has a form (Torrence and Compo, 1998, 2005):

$$\Psi_o(\eta)=\pi^{-1/4}e^{i\omega_o\eta}e^{-\eta^2/2} \tag{5}$$

where: ω_o – nondimensional frequency, in the paper it is equal to 6 (Torrence and Compo, 1998, 2005).

In Eq. 4 the parameter s assigns the frequency, whereas the parameter t identifies the time around which the assigned frequencies are investigated. The wavelet power spectrum is presented in the form of three dimensional map, where the horizontal axis shows the values of parameter t, while the vertical axis shows the values of parameter s (frequencies). The values of wavelet power spectrum $|W(t,s)|^2$ are presented as an altitude. The wavelet power spectrum allows us to observe the changes of each frequency in time. In Fig.8 the contour plots of the wavelet power spectrums for selected bubble paths have been presented. The areas containing the highest value of $|W(t,s)|^2$ are filled with a grey color.

The changes of location of maximum values of $|W(t,s)|^2$ identify the changes of the dominant frequency in time. The wavelet power spectrum shows in what period of time of the pressure time series these frequencies appear.

In Fig. 8g it has been shown the wavelet power spectrum for test path. Because the value of $|W(t,s)|^2$ depends on the amplitude and frequency of data, therefore the $|W(t,s)|^2$ obtained for test path clearly identifies the oscillation frequency only when the amplitude of oscillations is enough large. It happens in certain distance from the nozzle outlet. The higher value of $|W(t,s)|^2$ have been market in Fig. 8 with grey color.

The length of the area marked with grey color is a measure of time in which the oscillatory bubble movement with frequency about 5 [Hz] is stable. The length of grey area decreases together with the increase of frequency of bubble departures.

3.1. Attractor reconstruction

In order to qualitatively describe the stability of oscillatory movement of bubbles the non-linear analysis with using the recurrence plot method has been carried out.

The trajectories of the chaotic system in the phase space do not form any single geometrical object such as circle or torus, but form objects called strange attractors of the structure resembling the one of a fractal [8]. Non linear analysis starts from attractor reconstruction. Reconstruction of attractor in certain embedding dimension has been carried out using the stroboscope coordination. In this method subsequent co-ordinates of attractor points are calculated basing on the subsequent samples distant of time delay τ. The time delay is multiplication of time between the samples. The image of the attractor in n-dimensional space depends upon time-delay τ. When the time-delay is too small, the attractor gets flattened, that makes further analysis of its structure impossible. The selection of time-delay value is of great significance in the analysis of the attractor properties.

Therefore the analysis of the experimental data is initiated by determining the time-delay. For that purpose the autocorrelation function is calculated. Autocorrelation function allows identification of correlation between the subsequent samples. In case of chaotic data the value of autocorrelation function rapidly decrease when τ increase. Value of the time-delay τ is determined from the condition $C(\tau)\approx 0.5*C(0)$ (Schuster, 1993).

In Fig. 9 it has been shown the 3D attractor reconstruction obtained for time delay calculated using the mutual information method. For the low frequency of bubble departure (Fig. 9a,b,c) the spiral structure of attractor is visible. For the high frequency of bubble departure (Fig. 9d) the spiral structure of attractor is invisible.

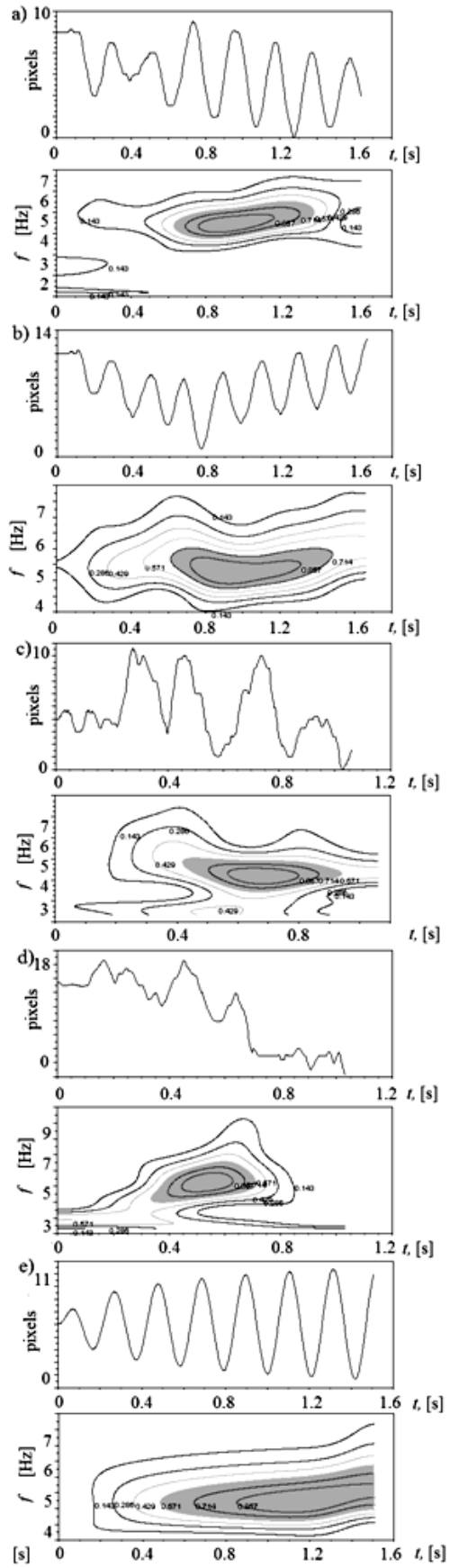

Fig. 8. Bubble paths and wavelet power spectrums for different frequencies of bubble departures f_b. a) f_b = 0.9 Hz, b) f_b = 4.1 Hz, c) f_b = 31.7 Hz, d) f_b = 36.5 Hz, e) Test path

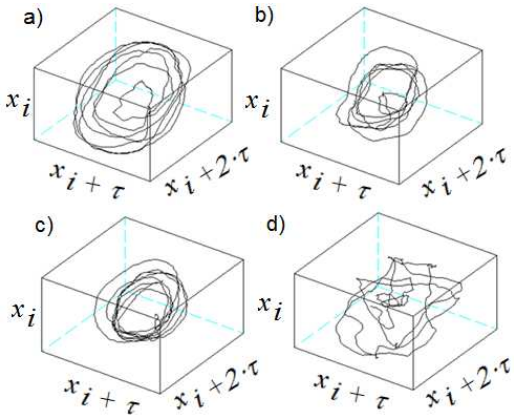

Fig. 9. 3D attractor reconstructions for different frequencies of bubble departures f_b. a) f_b = 0.9 [Hz], b) f_b = 2.9 [Hz], c) f_b = 4.1 [Hz], e) f_b = 31.7 [Hz]

3.2. Recurrence plot

Recurrence plot (RP) visualize the recurrence of states x_i in a phase space. The RP enables us to investigate the recurrence of state in m-dimensional phase. The recurrence of a state at time i at a different time j is marked within black dots in the plot, where both axes are time axes. From the formal point of view the RP can be expressed as Marwan et al. (2007):

$$R_{i,j} = \Theta\left(\varepsilon_i - \left\|x_i - x_j\right\|\right),\ x_i \in \Re^m,\ i,j - 1 \ldots N \qquad (6)$$

where N is the number of considered states x_i, ε_i is a threshold distance, $\|\ \|$ a norm and Θ the Heaviside function.

Homogeneous RPs are typical for stationary systems in which relaxation times are short in comparison with the time of system investigation. Oscillating systems have RPs with diagonal oriented, periodic recurrent structures. For quasi-periodic systems, the distances between the diagonal lines are different. The drift is caused by systems with slowly varying parameters which cause changes of brightens of the RP's upper-left and lower-right corners. Abrupt changes in the dynamics as well as extreme events cause white areas or bands in the RP (Marwan et al., 2007).

In Fig. 10 the RPs obtained for different frequencies of bubble departure have been presented. The RP has been made for 2D attractor reconstruction and ε equal to 1% of maximal lateral bubble displacement. For each frequency of bubble departure the time series of bubble lateral displacement (upper part of figure) and RP (lower part of figure) have been shown. In Fig. 10f it has been presented the RP prepared for the test time series where $x(t) = \ln(t) \cdot \sin(\omega \cdot t)$. The distance between parallel diagonal lines identifies the time series period. The distance between parallel diagonal lines in RP (Fig. 10a,b) is a result from the period of function of bubble lateral displacement and is equal to ~80 points (about 5 [Hz]) (Marwan et al., 2007).

The recurrence rate (*RR*) represents the percentage of recurrence points in RP (Marwan et al., 2007). The recurrence rate corresponds to the correlation sum (Marwan et al., 2007). The number of recurrence points increases with increase of frequency of bubble departure (Mosdorf and Wyszkowski, 2010). Because all recurrence plots have been constructed basing on a single bubble trajectory, there-

fore the increase of *RR* is a result of increase of complexity of attractors.

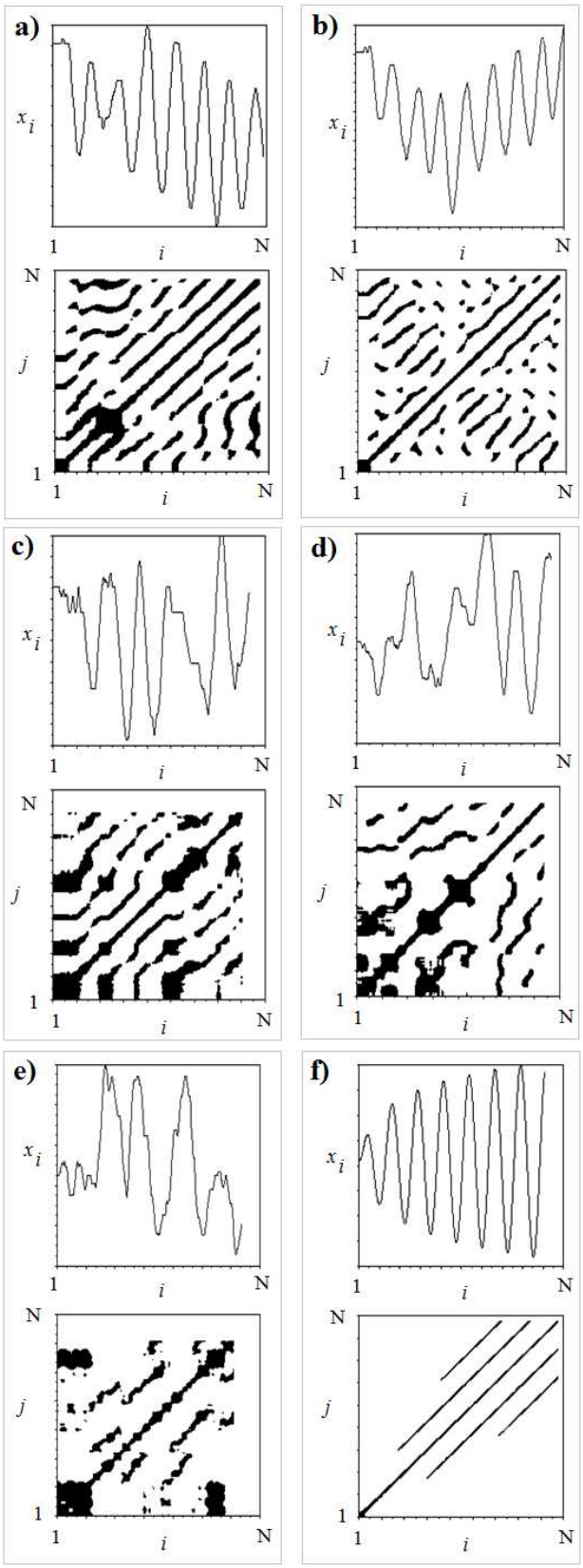

Fig. 10. Recurrence plots for different frequencies of bubble departures f_b. a) f_b = 0.9 [Hz], b) f_b = 4.1 [Hz], c) f_b = 13.6 [Hz], d) f_b = 17.2 [Hz], e) f_b = 31.7 [Hz], f) Test path

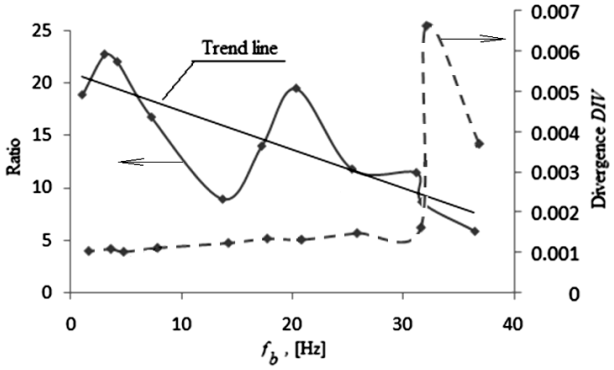

Fig. 11. The inverse of L_{max} (*DIV*) and the ratio between *DET* and *RR*

A diagonal line occurs in the RP when a segment of the trajectory runs parallel to another segment and the distance between trajectories is less than ε. The length of this diagonal line is determined by the duration of this phenomenon. Determinism (*DET*) is a percentage of recurrence points which form diagonal lines (Marwan et al., 2007). The *DET* can be treated as a measure of disappearance of spiral shape of the attractor.

Ratio coefficient *RATIO* is a ratio of *DET* to *RR* defined as Marwan et al. (2007):

$$RATIO = N^2 \frac{\sum_{l=l_{min}}^{N} lP(l)}{(\sum_{l=1}^{N} lP(l))} \tag{7}$$

In Fig. 11 the RATIO vs frequency of bubble departure has been show. For frequency of bubble departures less than 30 [Hz] the coefficient *RATIO* oscillates around the trend line. The oscillations become small for f_b > 30 [Hz]. Obtained results indicate that effect of interaction between subsequent bubbles which destroy the spiral motion of the bubble can be detected by coefficient *RATIO* for frequencies of bubble departure greater than 30 [Hz]. Before these frequency the large fluctuation around the trend line are observed.

The longest diagonal line L_{max} determines the mean vertical length of bubble path where the phenomenon of stability loss does not cause the rapid changes in bubbles path character. The inverse of L_{max} is defined as Marwan et al. (2007):

$$DIV = \frac{1}{L_{max}} \tag{8}$$

and it is related with the *KS* entropy of the system, i.e. with the sum of the positive Lyapunov exponents (Marwan et al., 2007). In Fig. 11 it has been shown the function of DIV vs frequency of bubble departure.

The positive Lyapunov exponents is a measure of instability of system trajectory. Obtained results show that bubble paths become more unstable when bubble departure frequency increases. The rapid increase of instability of bubble paths is observed for bubble departure frequency greater than 30 [Hz].

4. CONCLUSIONS

In the paper the paths of bubbles emitted from the nozzle with frequency of bubble departures which ranged from

1 to 36 Hz have been analyzed. The frequency analysis and recurrence plots have been used to determine the strength of interaction between bubbles in the bubble chain.

The wavelet analysis shows that the time of stable oscillatory bubble movement with oscillation frequency about 5 [Hz] decreases together with the increase of bubble departures frequency. Qualitative analysis of this phenomenon prepared with using the Recurrence Plot method has shown that–the increase of frequency of bubble departure causes decrease of number of the recurrence points which form diagonal lines. This confirms that periodic character of oscillatory trajectory disappears with the increase of frequency of bubble departure. The length of the longest diagonal line can be used to estimate the stability of bubble trajectory. It has been found that the rapid increase of instability of bubble paths is observed for bubble departure frequency greater than 30 [Hz].

The average length of the vertical lines of RP indicates a time in which a bubble trajectory changes very slowly. This time is equals to ~0.05 s and corresponds to time delay obtained using the minimum mutual information method.

It has been found that the rapid increase of instability of bubble paths is observed for bubble departure frequency greater than 30 [Hz]. In this case the distance between subsequent departing bubbles (*S/D*) becomes close to 1. It causes that the vertical interaction between departing bubbles is enough strong to change the dynamical properties of bubble paths.

REFERENCES

1. **Femat R., Ramirez J. A., Soria A.** (1998), Chaotic flow structure in a vertical bubble column, *Physics Letters A*, 248, 67-79.
2. **Hedengren, K. H.** (1988), Pattern Recognition, *9th International Conference on 14-17 Nov. 1988*, vol. 2, 963 – 965.
3. **Kikuchi R. et al.** (1997), Diagnosis of chaotic dynamics of bubble motion in a bubble column, *Chemical Engng Sc.*, 52, 3741-3745.
4. **Luewisutthichat W., Tsutsumi A., Yoshida K.** (1997), Chaotic hydrodynamics of continuous single-bubble flow system, *Chemical Engng Sc.*, 52, 3685-3691.
5. **Marwan N., Romano M. C., Thiel M., Kurths J.** (2007), Recurrence Plots for the Analysis of Complex Systems, *Physics Reports*, 438 (5-6), 237-329, Recurrence Plots And Cross Recurrence Plots (www.recurrence-plot.tk).
6. **Mosdorf R., Shoji M.** (2003), Chaos in bubbling – nonlinear analysis and modelling, *Chemical Engng Sc.*, 58, 3837-3846.
7. **Mosdorf R., Wyszkowski T.** (2010), *Using the Recurrence Plot in analysis of bubble paths in a bubble column*, CHISA 2010, CD version
8. **Schuster, H. G.** (1993), *Deterministic chaos*, An introduction, PWN, Warsaw (in Polish).
9. **Torrence C., Compo G. P.** (1998), A practical guide to wavelet analysis, *Bull. Am. Meteorolog. Soc.*, 79 (1).
10. **Torrence C., Compo G. P.** (2005), *A Practical Guide to Wavelet Analysis, with Significance and Confidence Testing*, Available from: http://paos.colorado.edu/research/wavelets/.
11. **Vazquez A., Manasseh R., Sánchez R. M., Metcalfe G.** (2008), Experimental comparison between acoustic and pressure signals from a bubbling flow, *Chemical Engineering Science*, 63, 5860-5869.
12. **Zenit R., Magnaudet J.** (2009), Measurements of the streamwise vorticity in the wake of an oscillating bubble, *International Journal of Multiphase Flow*, 35, 195–203.
13. **Zhang L., Shoji M.** (2001), Aperiodic bubble formation from submerged orifice, *Chemical Engng Sc.*, 56,5371-5381.

The authors are grateful for the financial support of Ministry of Science and Higher Education in Poland (Grant: N N503 138936).